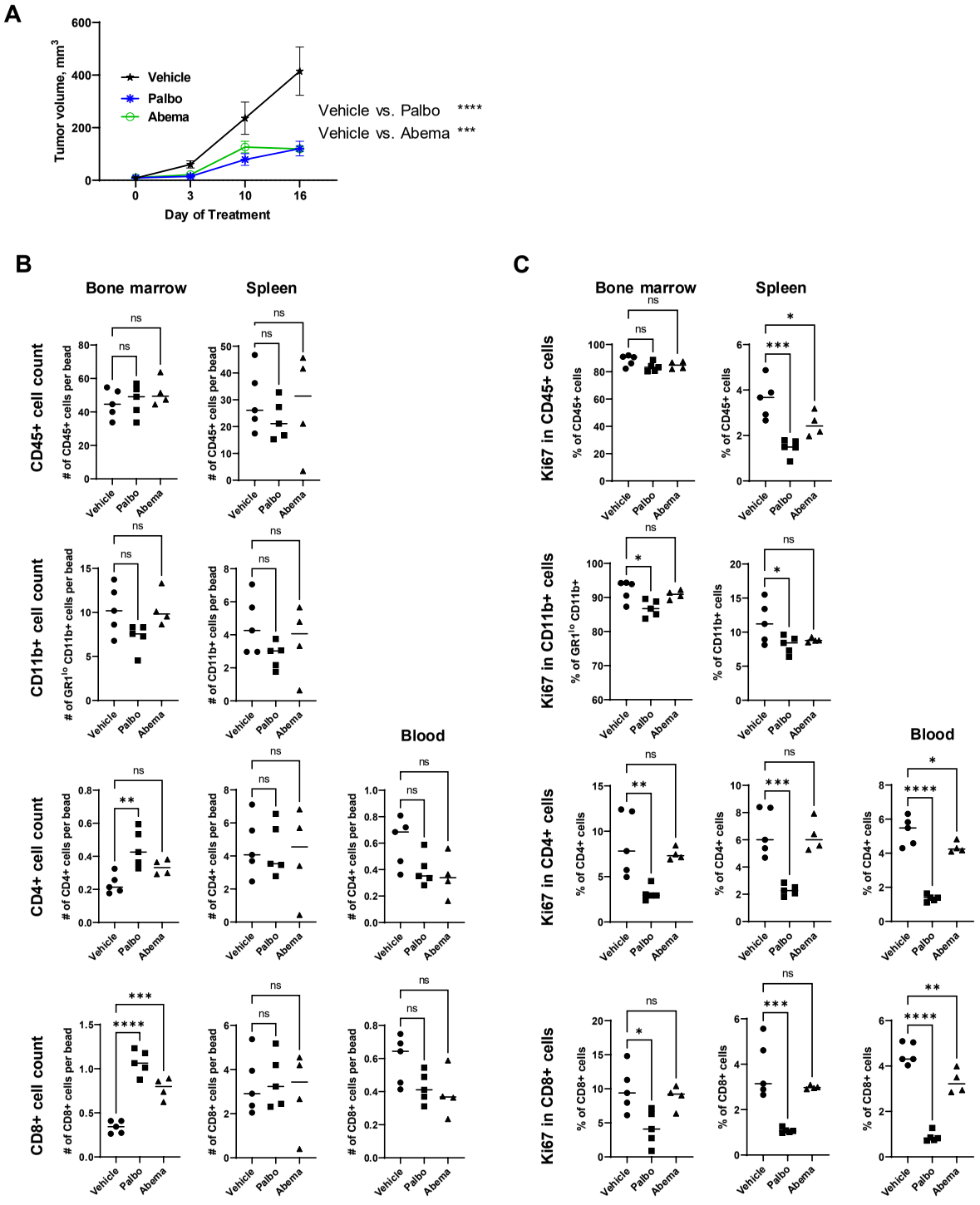

Figure S1

Kumar A, *et al. J Immunother Cancer* 2023; 11:e006019. doi: 10.1136/jitc-2022-006019

Figure S1: Effect of CDK4/6i-therapy on myeloid and lymphoid subsets in BM, spleen and peripheral blood. A-C. PYMT-tumor bearing mice were treated with palbociclib, abemaciclib or vehicle for 15 days. B-C. Single cells from BM, spleen and peripheral blood were isolated (see methods) followed by FACS staining to identify CD45+, CD11b+, CD4-T and CD8-T cells and monitor Ki67 expression on them. A. Tumor volume change over time, n's are Vehicle (n=5), palbociclib (n=5), abemaciclib (n=4). Statistical analysis using mixed model with Dunnett's post-test was performed to compare tumor growth in different treatment groups. B. Graphs showing relative numbers of indicated immune cell populations per 1 femur (bone marrow), entire spleen, or 1 mL of blood. Cell numbers were calculated as absolute number of cells in the gate of interest divided by the absolute number of counting beads. C. Dot plots showing % Ki67+ cells in indicated immune subsets. n's as in A. Statistical comparison between vehicle and treatment groups (palbociclib or abemaciclib) in B-C was performed using ANOVA with Dunnett's post-test. ns, not significant ($p \geq 0.05$), *p=0.01-0.05, **p=0.001-0.01, ***p=0.0001-0.001.

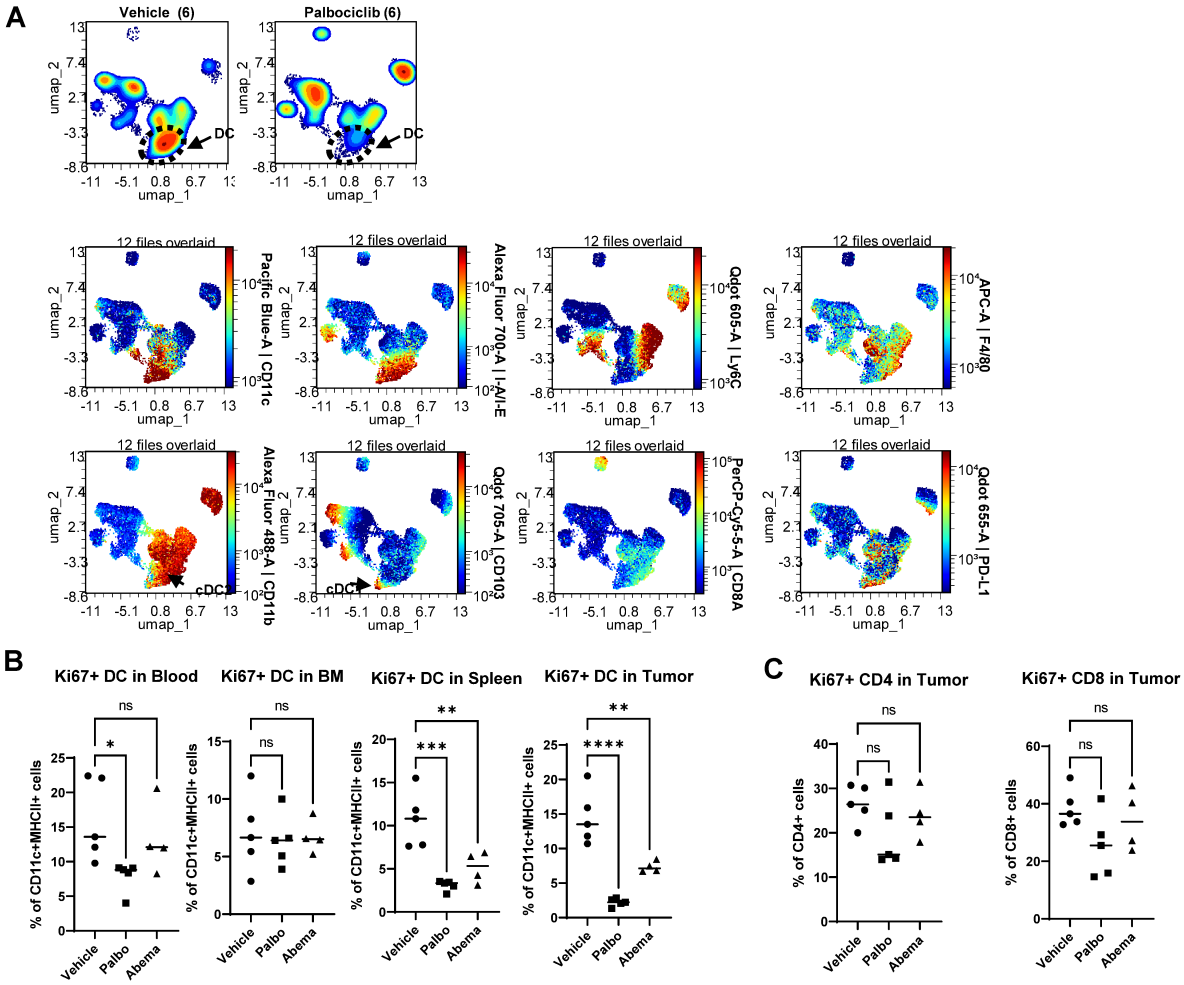
A
Vehicle (6)
Palbociclib (6)
DC
umap_1
umap_2
12 files overlaid
Pacific Blue-A | CD11c
Alexa Fluor 700-A | I-A/I-E
Qdot 605-A | Ly6C
APC-A | F4/80
Alexa Fluor 488-A | CD11b
Qdot 705-A | CD103
PerCP-Cy5-5-A | CD8A
Qdot 655-A | PD-L1
cDC1
B
Ki67+ DC in Blood
Ki67+ DC in BM
Ki67+ DC in Spleen
Ki67+ DC in Tumor
% of CD11c+MHCII+ cells
Vehicle
Palbo
Abema
ns
*
**
***
****
C
Ki67+ CD4 in Tumor
Ki67+ CD8 in Tumor
% of CD4+ cells
% of CD8+ cells

Figure S2

Figure S2. Palbociclib treatment inhibits dendritic cell in murine breast cancer model and *in vitro*. A. Mice were inoculated with PYMT-C57 cells and treated with 100 mg/kg palbociclib or vehicle QD for 4 weeks. N=5 mice per treatment group. The tumor cell suspension was analyzed for immune cell surface marker expression using flow cytometry. UMAP plots were constructed for multiparametrical representation of multicolor flow cytometry data. Top panels: Density UMAP plots showing immune cell distribution in concatenated vehicle and palbociclib specimens. Bottom panels: Tested marker expression (indicated on the right) across cell populations distributed on UMAP plots. Punctate outline and arrows indicate populations of total DCs, and their cDC1 and cDC2 subsets. B-C**.** Percentages of Ki67 positive cells within CD11c+ MHCII+ DC populations in indicated tissues from mice shown in S1A. Statistical analysis using ANOVA with Dunnett's post-test. *p=0.01-0.05, ***p=0.0001-0.001, ****p<0.0001.

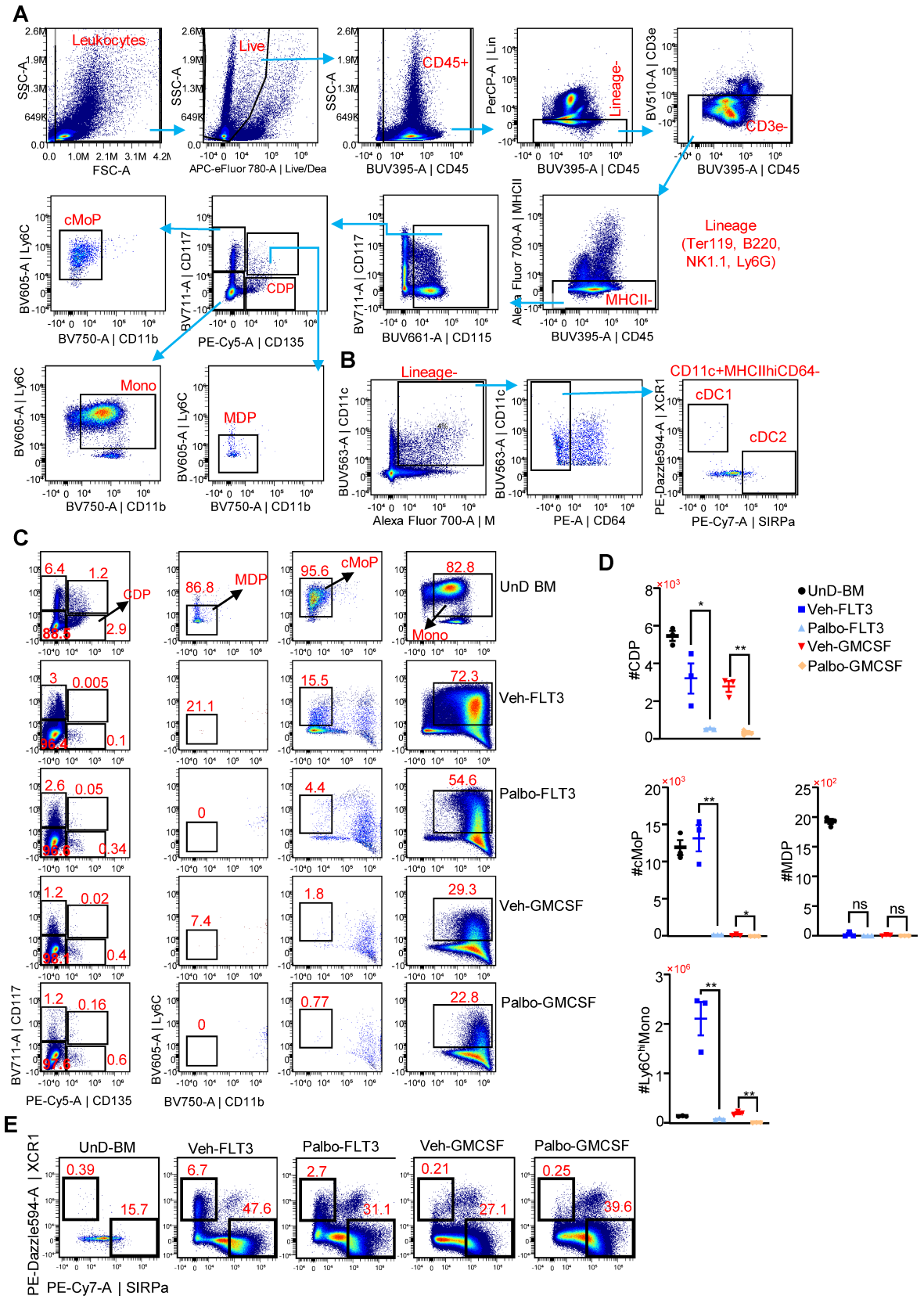
A
Leukocytes
Live
CD45+
Lineage-
CD3e-
Lineage (Ter119, B220, NK1.1, Ly6G)
MHCII-
cMoP
CDP
Mono
MDP
B
Lineage-
CD11c+MHCIIhiCD64-
cDC1
cDC2
C
UnD BM
Veh-FLT3
Palbo-FLT3
Veh-GMCSF
Palbo-GMCSF
D
UnD-BM
Veh-FLT3
Palbo-FLT3
Veh-GMCSF
Palbo-GMCSF
#CDP
#cMoP
#MDP
#Ly6C^hiMono
ns
E
UnD-BM
Veh-FLT3
Palbo-FLT3
Veh-GMCSF
Palbo-GMCSF
PE-Dazzle594-A | XCR1
PE-Cy7-A | SIRPa

Figure S3

Figure S3. CDK4/6i therapy suppresses DCs differentiation and proliferation *in vitro*. A-B. Strategy to gate DCs and monocyte precursors (A) and DC subsets (B). A. Live leukocytes were gated to identify CD45+ cells followed by lineage gating (lineage markers were Ter119, B220, NK1.1 and Ly6G). Lineage negative (Lineage-) cells were further gated to identify $CD3e^-$ cells followed by gating out $MHCII^+$ cells. $CD115^+$ and $CD115^+CD117^+$ cells were further gated to identify monocyte and DC progenitor (MDP), common DC progenitor (CDP), common monocyte progenitor (cMoP) and. $Ly6C^{hi}$ monocytes. B. $CD11c^+MHCII^{hi}$ cell were gated within the $CD45^+$ gate (as in A) followed by gating cDC1 ($XCR1^+$) and cDC2 ($SIRP\alpha^+$) DCs within $CD11c^+MHCII^{hi}$ gate. C-E. Murine bone marrow cells were cultured in the presence different culture condition with or without palbociclib as in Fig. 3H (see also methods). DC and monocyte precursor (C-D) and DC subsets (E) were identified as in A. C. Representative (of 3-independent experiments) FACS plots showing frequencies of indicated population. D. Dot plot showing total numbers of indicated DC precursors (determined from their frequencies and total BMDCs harvested). E. Representative (of three independent experiments) FACS plots showing frequencies of cDC1 and cDC2 subsets. ns, not significant ($p \geq 0.05$), *p=0.01-0.05, **p=0.001-0.01.

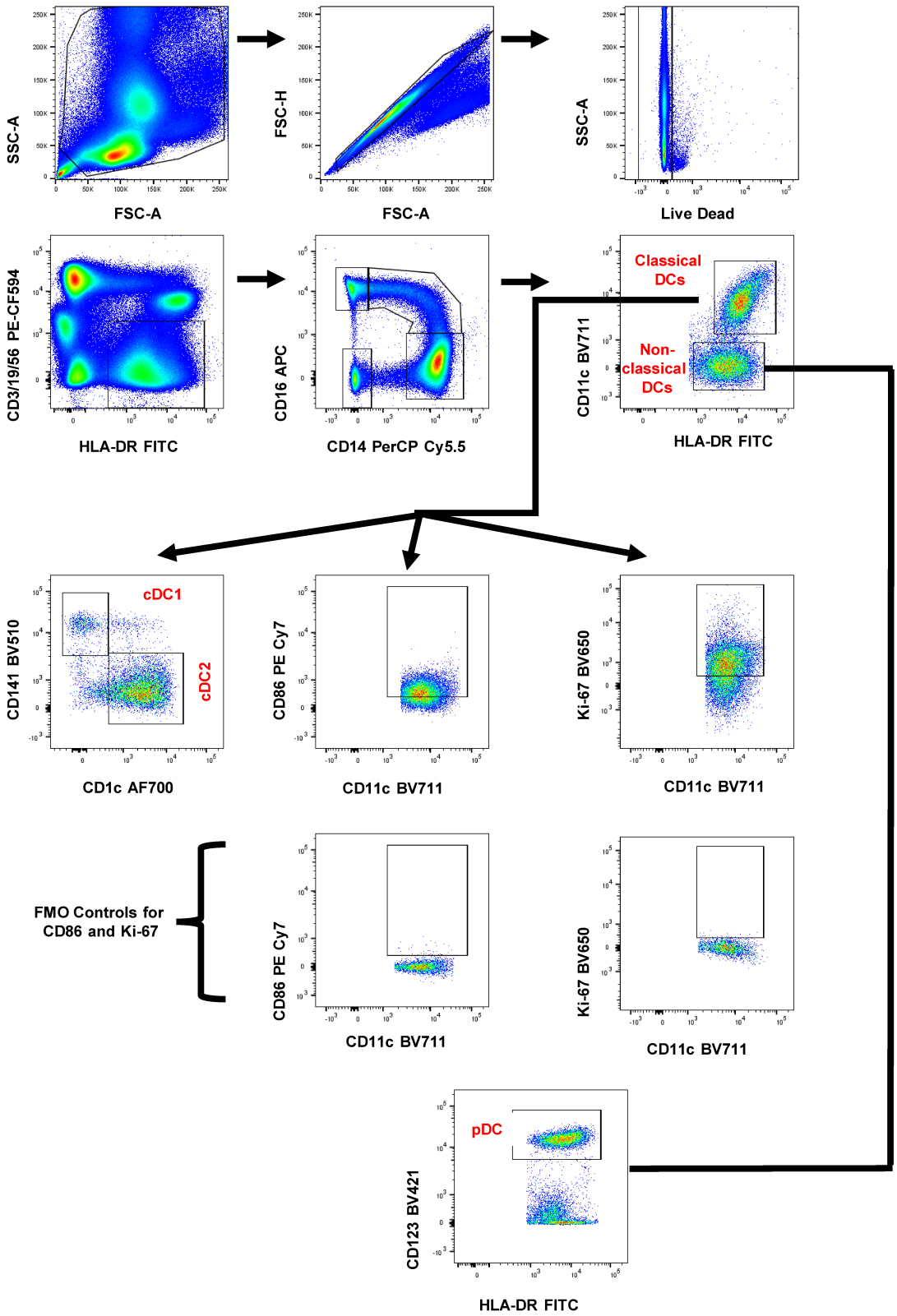
SSC-A
FSC-A
FSC-H
FSC-A
SSC-A
Live Dead
CD3/19/56 PE-CF594
HLA-DR FITC
CD16 APC
CD14 PerCP Cy5.5
Classical DCs
Non-classical DCs
CD11c BV711
HLA-DR FITC
cDC1
cDC2
CD141 BV510
CD1c AF700
CD86 PE Cy7
CD11c BV711
Ki-67 BV650
CD11c BV711
FMO Controls for CD86 and Ki-67
CD86 PE Cy7
CD11c BV711
Ki-67 BV650
CD11c BV711
pDC
CD123 BV421
HLA-DR FITC

Figure S4

Figure S4. Strategy to gate peripheral blood mononuclear cells for dendritic cell populations. Flow cytometric plots illustrate gating for cells from FSC-A and SSC-A → single cells from FSC-A and FSC-H → live cells from single cells based on Live Dead stain → antigen-presenting cells by cell lineage (CD3/19/56/NK/220) exclusion and HLA-DR+ → dendritic cells from double negative non-monocytic cells vs. monocytic populations gated based on CD14+/CD16- (classical monocytes, CD14+/CD16+ (atypical monocytes), CD14-/CD16+ (non-classical monocytes) → within dendritic cells CD11c and HLA DR+ double positive defined as conventional dendritic cells → CD141+ as cDC1 and CD1c+ as cDC2. Activation and proliferation gates were determined based on FMO controls. For plasmacytoid dendritic cells, CD11c- cells were subsequently gated on CD123+.

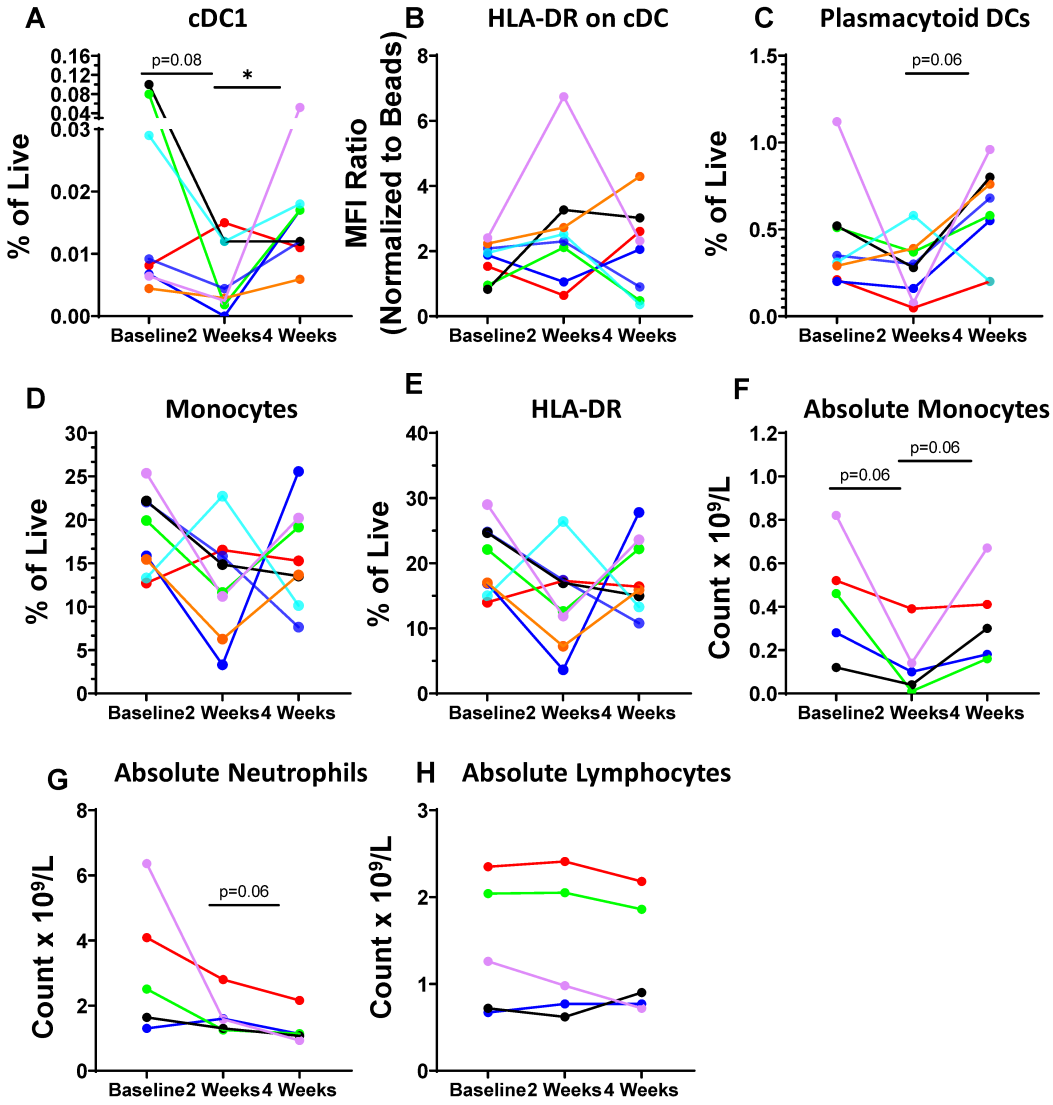
A
cDC1
% of Live
p=0.08
*
Baseline2 Weeks4 Weeks
B
HLA-DR on cDC
MFI Ratio (Normalized to Beads)
Baseline2 Weeks4 Weeks
C
Plasmacytoid DCs
% of Live
p=0.06
Baseline2 Weeks4 Weeks
D
Monocytes
% of Live
Baseline2 Weeks4 Weeks
E
HLA-DR
% of Live
Baseline2 Weeks4 Weeks
F
Absolute Monocytes
Count x 10⁹/L
p=0.06
p=0.06
Baseline2 Weeks4 Weeks
G
Absolute Neutrophils
Count x 10⁹/L
p=0.06
Baseline2 Weeks4 Weeks
H
Absolute Lymphocytes
Count x 10⁹/L
Baseline2 Weeks4 Weeks

Figure S5

Figure S5. Palbociclib decreases cDC1, monocytes, and HLA-DR+ antigen-presenting cells without changing absolute lymphocyte number in the blood of patients with metastatic hormone receptor-positive breast cancer. A. Longitudinal change in cDC1 cells as expressed by percentage of live cells by flow cytometry. **B.** Change in HLA-DR expression on conventional dendritic cells as measured by mean fluorescence intensity of sample normalized to beads. **C-E.** Longitudinal changes in plasmacytoid dendritic cells, monocytes, and HLA-DR+/lineage negative cells with all expressed as a percentage of live cells by flow cytometry. **F-H.** Longitudinal change in absolute monocyte, neutrophil, and lymphocyte counts as measured on clinical complete blood counting tests. Different patients are represented by unique colors corresponding to them throughout the plots. Longitudinal changes were assessed by the Wilcoxon matched-pairs signed rank test, and significant results were indicated with * ($p<0.05$).

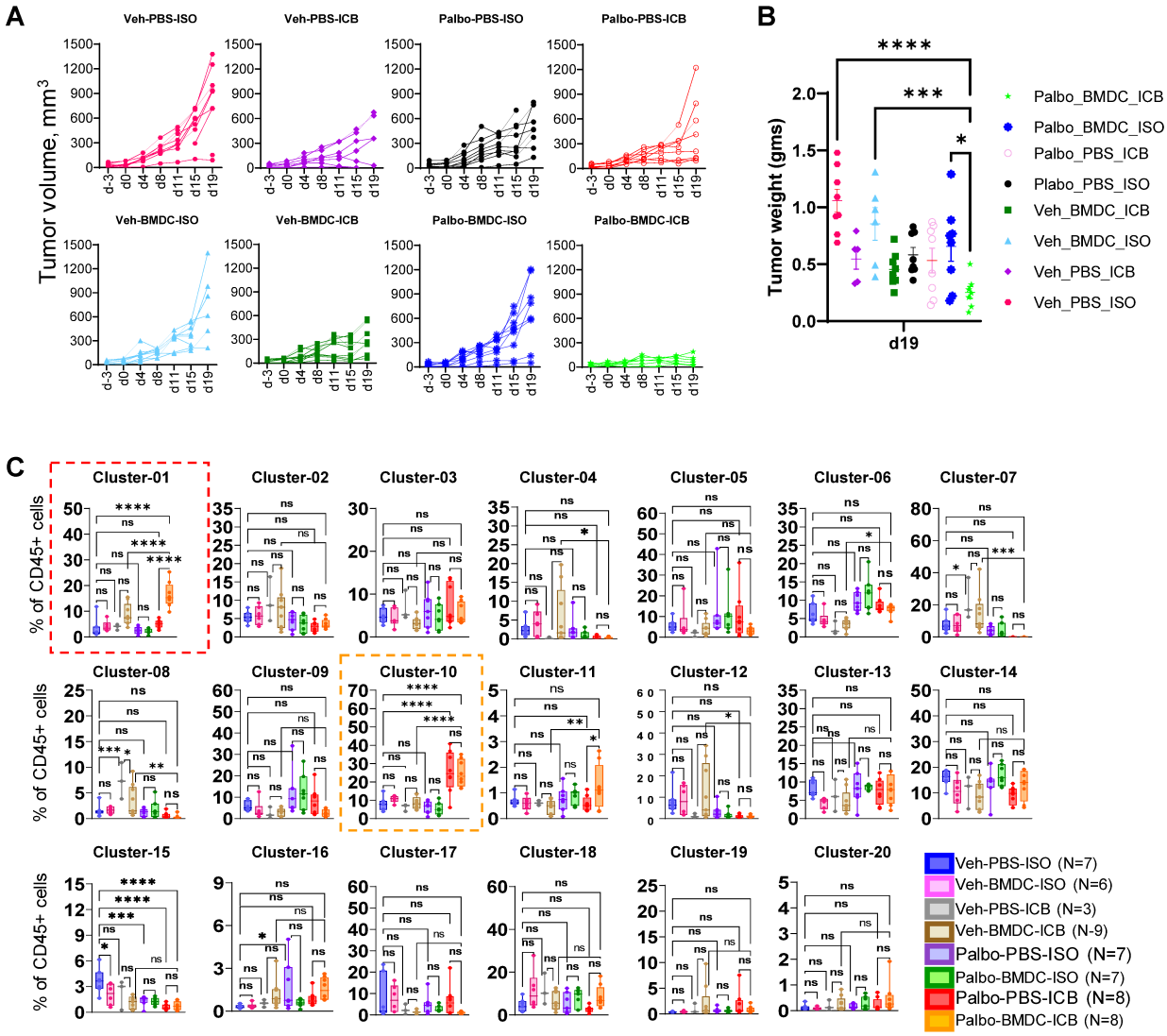
A
Veh-PBS-ISO
Veh-PBS-ICB
Palbo-PBS-ISO
Palbo-PBS-ICB
Veh-BMDC-ISO
Veh-BMDC-ICB
Palbo-BMDC-ISO
Palbo-BMDC-ICB
Tumor volume, mm3
B
Tumor weight (gms)
d19
Palbo_BMDC_ICB
Palbo_BMDC_ISO
Palbo_PBS_ICB
Plabo_PBS_ISO
Veh_BMDC_ICB
Veh_BMDC_ISO
Veh_PBS_ICB
Veh_PBS_ISO
C
% of CD45+ cells
Cluster-01
Cluster-02
Cluster-03
Cluster-04
Cluster-05
Cluster-06
Cluster-07
Cluster-08
Cluster-09
Cluster-10
Cluster-11
Cluster-12
Cluster-13
Cluster-14
Cluster-15
Cluster-16
Cluster-17
Cluster-18
Cluster-19
Cluster-20
Veh-PBS-ISO (N=7)
Veh-BMDC-ISO (N=6)
Veh-PBS-ICB (N=3)
Veh-BMDC-ICB (N-9)
Palbo-PBS-ISO (N=7)
Palbo-BMDC-ISO (N=7)
Palbo-PBS-ICB (N=8)
Palbo-BMDC-ICB (N=8)
D
Cluster 1 phenotype (PD-1-/CD4+)
Cluster 10 phenotype (PD-1-/CD8+)
% of live cells
Vehicle_PBS_ISO
Vehicle_PBS_ICB
Vehicle_BMDC_ISO
Vehicle_BMDC_ICB
Palbociclib_PBS_ISO
Palbociclib_PBS_ICB
Palbociclib_BMDC_ISO
Palbociclib_BMDC_ICB

Figure S6

Figure S6. The CDK4/6i, ICB, and BMDC therapy promotes favorable tumor immune microenvironment in a murine breast cancer model. A-C. PYMT tumor-bearing mice were treated with palbociclib or vehicle control and received two i.v. injections of 5×10^6 BMDCs on d1 and d8. Immunotherapy (CTLA-4 and PD-1 antibodies) or isotype controls at 100 µg/mouse for each antibody were administered on d1, d5, d8, d11, and d15. **A**. Spaghetti plot showing tumor volume change over time (experimental schema described in Fig 5A; N=8-10 mice per treatment group on days 0-d17 and N=5-8 mice per treatment group on d19). B. Tumor weight measurements; N=5-8 mice per treatment group. Statistical comparison between treatment groups was performed using one-way ANOVA with Tukey's post-test with adjustment for multiple comparisons. Significance results (p values) are tabulated **C.** $CD45^+$ cells were clustered as described in Fig 5 and methods. Box plots showing cluster frequencies in each treatment group. D. Graphs showing frequencies of cells with cluster 1-like phenotype ($PD\text{-}1^-/CD4^+$) and cluster 10-like phenotype ($PD\text{-}1^-/CD8^+$) within live tumor cells. Statistical comparison between treatment groups was performed using one-way ANOVA with Dunnett's post-test with adjustment for multiple comparisons. ns, not significant ($p\geq0.05$), *p=0.01-0.05, **p=0.001-0.01, ***p=0.0001-0.001, ****$p<0.0001$.

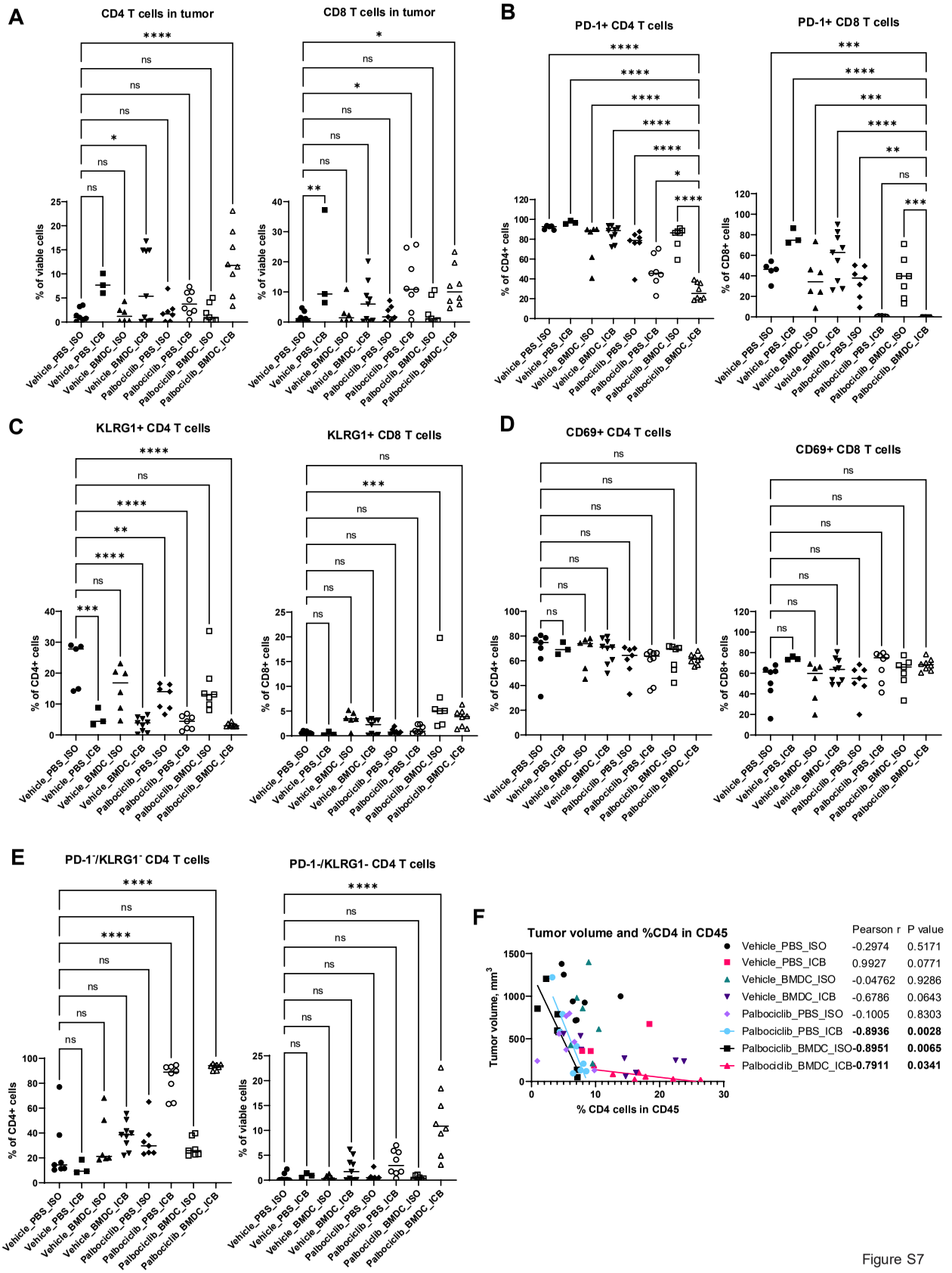

Figure S7

Kumar A, *et al*. *J Immunother Cancer* 2023; 11:e006019. doi: 10.1136/jitc-2022-006019

Figure S7. The CDK4/6i, ICB, and BMDC therapy enhance abundance of PD-1$^-$/KLRG1$^-$ CD4 T cells in TME. A-F. Analysis of CD4 and CD8 T cells in PYMT tumors from mice shown in Fig S6. A Graphs showing percentage CD4-T (left) and CD8-T within viable tumor cells in indicated treatment groups, n's as shown Fig. S6C (parenthesis). **B-D**. Graphs showing percentages of PD-1 (B), KLRG1 (C) and CD69 (D) expressing CD4-T and CD8-T cells (as % of CD4-T and CD8-T respectively) in indicated treatment groups, n's as in Fig S6C. **E**. Graphs showing frequency of PD-1$^-$KLRG1$^-$ CD4-T expressed as % of CD4 (left) and % of viable/live (right) cells, n's as in Fig S6C. F. Pearson correlation coefficient showing correlation (pearson r) between tumor volume on d19 (day of tumor harvesting) and percentage of CD4-T cells in CD45 cells from tumors. Statistical comparison was performed using one-way ANOVA with Dunnett's post-test with adjustment for multiple comparisons. ns, not significant ($p \geq 0.05$), *p=0.01-0.05, **p=0.001-0.01, ***p=0.0001-0.001, ****p<0.0001.

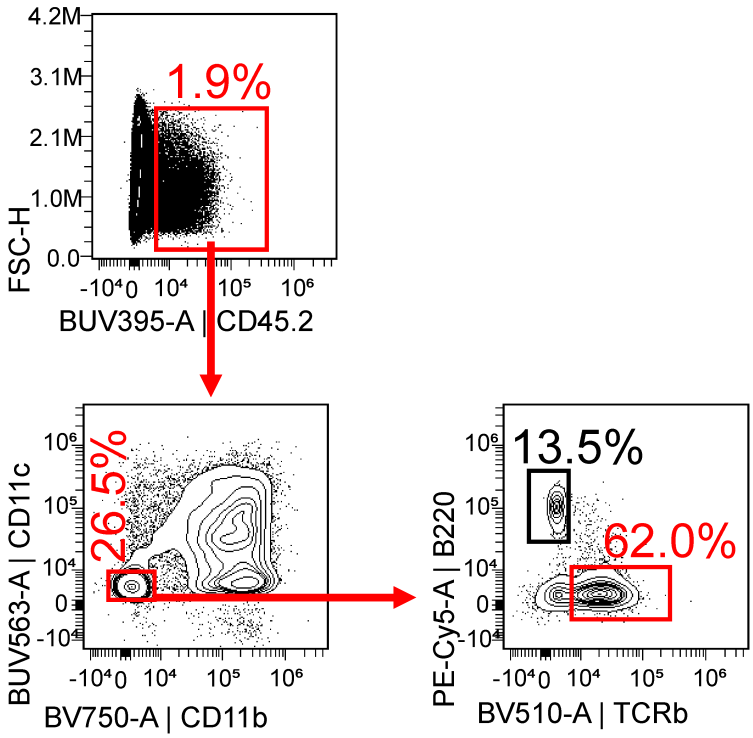
4.2M
3.1M
2.1M
1.0M
0.0
FSC-H
1.9%
-10⁴ 0 10⁴ 10⁵ 10⁶
BUV395-A | CD45.2
10⁶
10⁵
10⁴
0
-10⁴
BUV563-A | CD11c
26.5%
-10⁴ 0 10⁴ 10⁵ 10⁶
BV750-A | CD11b
13.5%
62.0%
PE-Cy5-A | B220
BV510-A | TCRb

Figure S8

Figure S8. Strategy to gate TCRβ+ T cells for dimensionality reduction and cluster analysis using OMIQ. The tumor cell suspensions were analyzed for immune cell marker expression using spectral flow cytometry. CD45+ cells were gated within live cells, followed by gating to identify CD11b-CD11c- cells. The CD11b-CD11c- cells were further gated to identify TCRβ+ T cells.

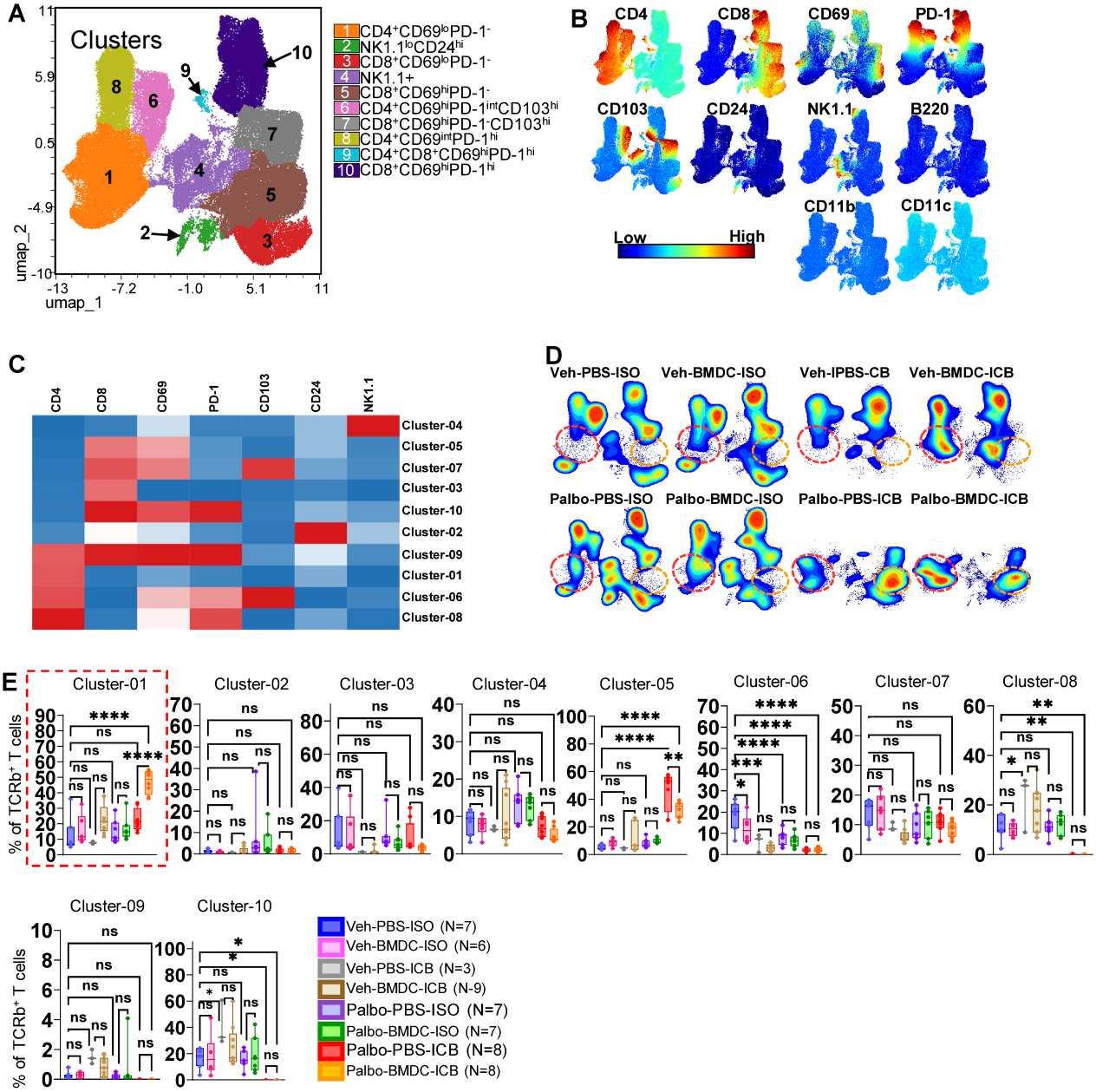
A
Clusters
1 CD4+CD69loPD-1-
2 NK1.1loCD24hi
3 CD8+CD69loPD-1-
4 NK1.1+
5 CD8+CD69hiPD-1-
6 CD4+CD69hiPD-1intCD103hi
7 CD8+CD69hiPD-1-CD103hi
8 CD4+CD69intPD-1hi
9 CD4+CD8+CD69hiPD-1hi
10 CD8+CD69hiPD-1hi
umap_1
umap_2
B
CD4
CD8
CD69
PD-1
CD103
CD24
NK1.1
B220
CD11b
CD11c
Low
High
C
CD4
CD8
CD69
PD-1
CD103
CD24
NK1.1
Cluster-04
Cluster-05
Cluster-07
Cluster-03
Cluster-10
Cluster-02
Cluster-09
Cluster-01
Cluster-06
Cluster-08
D
Veh-PBS-ISO
Veh-BMDC-ISO
Veh-IPBS-CB
Veh-BMDC-ICB
Palbo-PBS-ISO
Palbo-BMDC-ISO
Palbo-PBS-ICB
Palbo-BMDC-ICB
E
Cluster-01
Cluster-02
Cluster-03
Cluster-04
Cluster-05
Cluster-06
Cluster-07
Cluster-08
Cluster-09
Cluster-10
% of TCRb+ T cells
Veh-PBS-ISO (N=7)
Veh-BMDC-ISO (N=6)
Veh-PBS-ICB (N=3)
Veh-BMDC-ICB (N-9)
Palbo-PBS-ISO (N=7)
Palbo-BMDC-ISO (N=7)
Palbo-PBS-ICB (N=8)
Palbo-BMDC-ICB (N=8)

Figure S9

Figure S9. The CDK4/6i, ICB, and BMDC therapy enhances the abundance of activated CD4 T cells in TME. A-E. The tumor cell suspensions from indicated groups were analyzed for immune cell markers expression using spectral flow cytometry, and data was analyzed using OMIQ software (groups and N's as shown in E (parenthesis). UMAP plots were constructed for multiparametrical representation of multicolor flow cytometry data using concatenated data including 2000 cells per each individual sample. **A.** TCRβ^+ T cells were clustered using consensus clustering method to identify 10 distinct T cell populations and visualized on UMAP space. A total of 55 samples from all groups were concatenated. **B.** Individual marker expression pattern in cell islands is visualized on UMAP space. **C.** Using median expression of flow cytometry markers, a cluster-by-marker heatmap was generated to annotate each cluster. **D.** Contour plots were used to visualize the density of clusters/immune cells throughout the regions of UMAP space. **E.** Box plots showing cluster frequencies in each treatment group. The p values in E were calculated using ANOVA with Tukey's post-test with adjustment for multiple comparisons. ns, not significant ($p \geq 0.05$), *p=0.01-0.05, **p=0.001-0.01, ***p=0.0001-0.001, ****$p < 0.0001$.

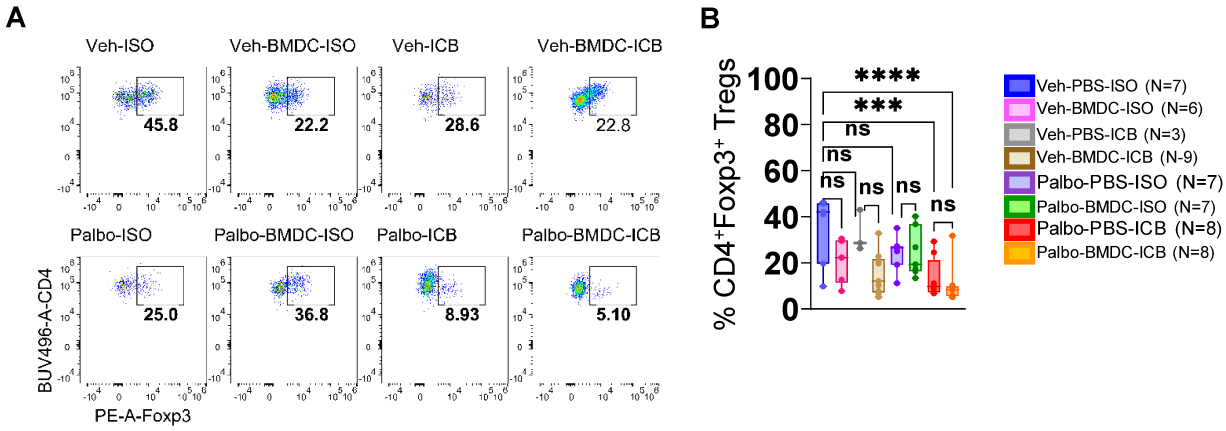
A
Veh-ISO
Veh-BMDC-ISO
Veh-ICB
Veh-BMDC-ICB
45.8
22.2
28.6
22.8
Palbo-ISO
Palbo-BMDC-ISO
Palbo-ICB
Palbo-BMDC-ICB
25.0
36.8
8.93
5.10
BUV496-A-CD4
PE-A-Foxp3
B
% CD4+Foxp3+ Tregs
100
80
60
40
20
0
****
***
ns
ns
ns
ns
ns
ns
Veh-PBS-ISO (N=7)
Veh-BMDC-ISO (N=6)
Veh-PBS-ICB (N=3)
Veh-BMDC-ICB (N-9)
Palbo-PBS-ISO (N=7)
Palbo-BMDC-ISO (N=7)
Palbo-PBS-ICB (N=8)
Palbo-BMDC-ICB (N=8)

Figure S10

Figure S10. The CDK4/6i and ICB therapy inhibits Tregs in TME. Representative FACS plots (**A)** and graphs (**B)** showing proportions of Foxp3+CD4+ cells in different treatment groups. N's as shown in parenthesis within the legend. The p values were calculated using ANOVA with Tukey's post-test with adjustment for multiple comparisons. ns, not significant ($p \geq 0.05$), *p=0.01-0.05, **p=0.001-0.01, ***p=0.0001-0.001, ****p<0.0001.

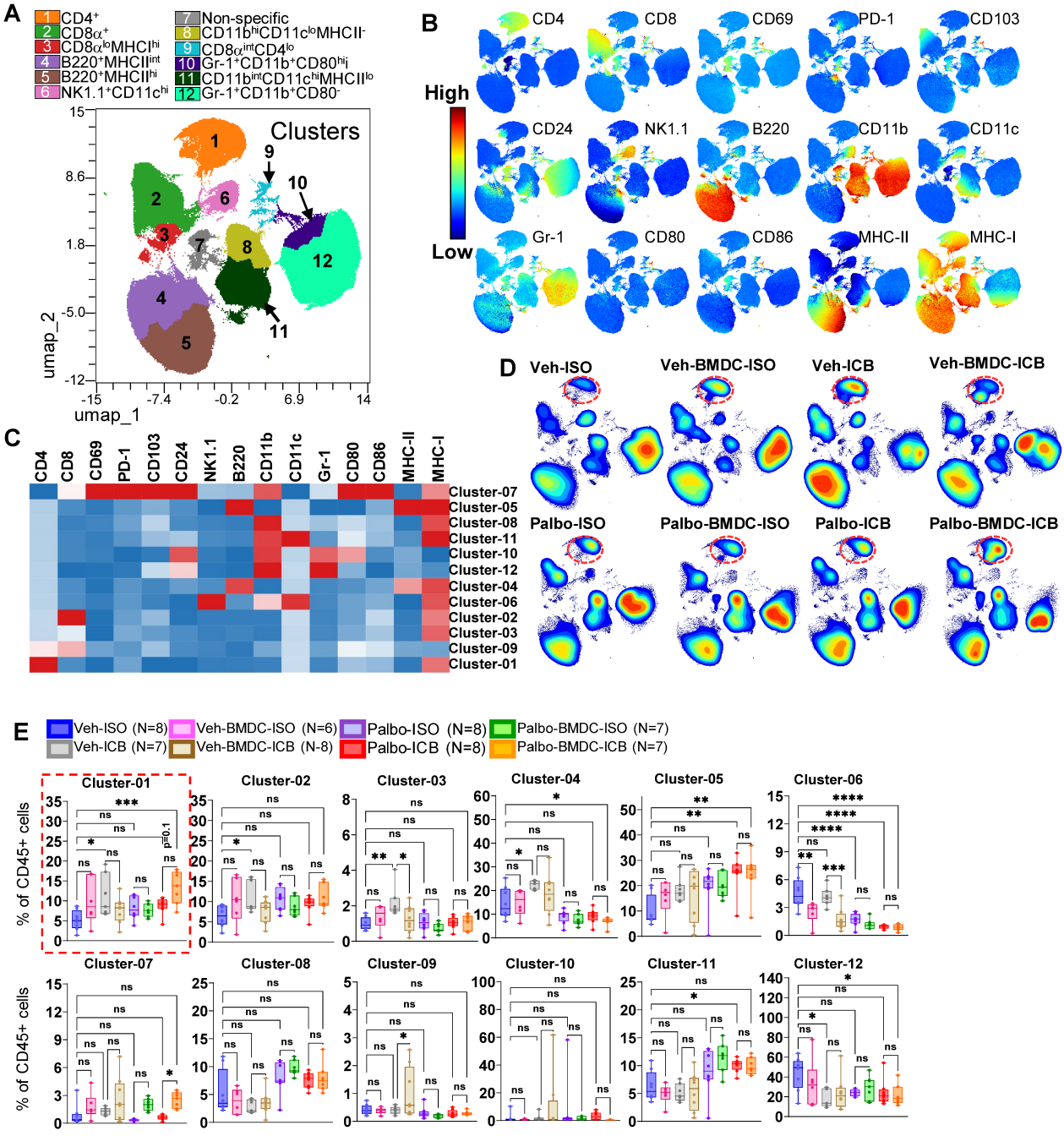
A
1 CD4+
2 CD8α+
3 CD8α^loMHCI^hi
4 B220+MHCII^int
5 B220+MHCII^hi
6 NK1.1+CD11c^hi
7 Non-specific
8 CD11b^hiCD11c^loMHCII-
9 CD8α^intCD4^lo
10 Gr-1+CD11b+CD80^hi
11 CD11b^intCD11c^hiMHCII^lo
12 Gr-1+CD11b+CD80-
Clusters
umap_1
umap_2
B
High
Low
CD4 CD8 CD69 PD-1 CD103
CD24 NK1.1 B220 CD11b CD11c
Gr-1 CD80 CD86 MHC-II MHC-I
C
CD4 CD8 CD69 PD-1 CD103 CD24 NK1.1 B220 CD11b CD11c Gr-1 CD80 CD86 MHC-II MHC-I
Cluster-07
Cluster-05
Cluster-08
Cluster-11
Cluster-10
Cluster-12
Cluster-04
Cluster-06
Cluster-02
Cluster-03
Cluster-09
Cluster-01
D
Veh-ISO
Veh-BMDC-ISO
Veh-ICB
Veh-BMDC-ICB
Palbo-ISO
Palbo-BMDC-ISO
Palbo-ICB
Palbo-BMDC-ICB
E
Veh-ISO (N=8)
Veh-BMDC-ISO (N=6)
Palbo-ISO (N=8)
Palbo-BMDC-ISO (N=7)
Veh-ICB (N=7)
Veh-BMDC-ICB (N-8)
Palbo-ICB (N=8)
Palbo-BMDC-ICB (N=7)
% of CD45+ cells
Cluster-01
Cluster-02
Cluster-03
Cluster-04
Cluster-05
Cluster-06
Cluster-07
Cluster-08
Cluster-09
Cluster-10
Cluster-11
Cluster-12

Figure S11

Figure S11. The CDK4/6i, ICB, and BMDC therapy enhances the abundance of activated CD4 T cells in peripheral blood. A-E. Peripheral blood immune cells were obtained by lysis of red blood cells. The single cell suspensions from indicated groups were analyzed for immune cell markers expression using high dimensional spectral flow cytometry and data was analyzed using OMIQ software (see methods for details; groups and N's as shown in E (parenthesis). UMAP plots were constructed for multiparametrical representation of multicolor flow cytometry data using concatenated data including 10000 cells per each individual sample. **A.** $CD45^+$ cells were clustered using consensus clustering method to identify 12 distinct immune cell clusters and visualized on UMAP space. A total of 55 samples from all groups were concatenated. **B.** Individual marker expression pattern in cell islands is visualized on UMAP space. **C.** Heatmap shows a median expression of flow cytometry markers in individual cell clusters. **D.** Contour plots were used to visualize the density of clusters/immune cells throughout the regions of UMAP space. **E.** Box plots showing cluster frequencies in each treatment group. The p values were calculated using ANOVA with Tukey's post-test with adjustment for multiple comparisons. ns, not significant ($p \geq 0.05$), *p=0.01-0.05, **p=0.001-0.01, ***p=0.0001-0.001, ****p<0.0001.

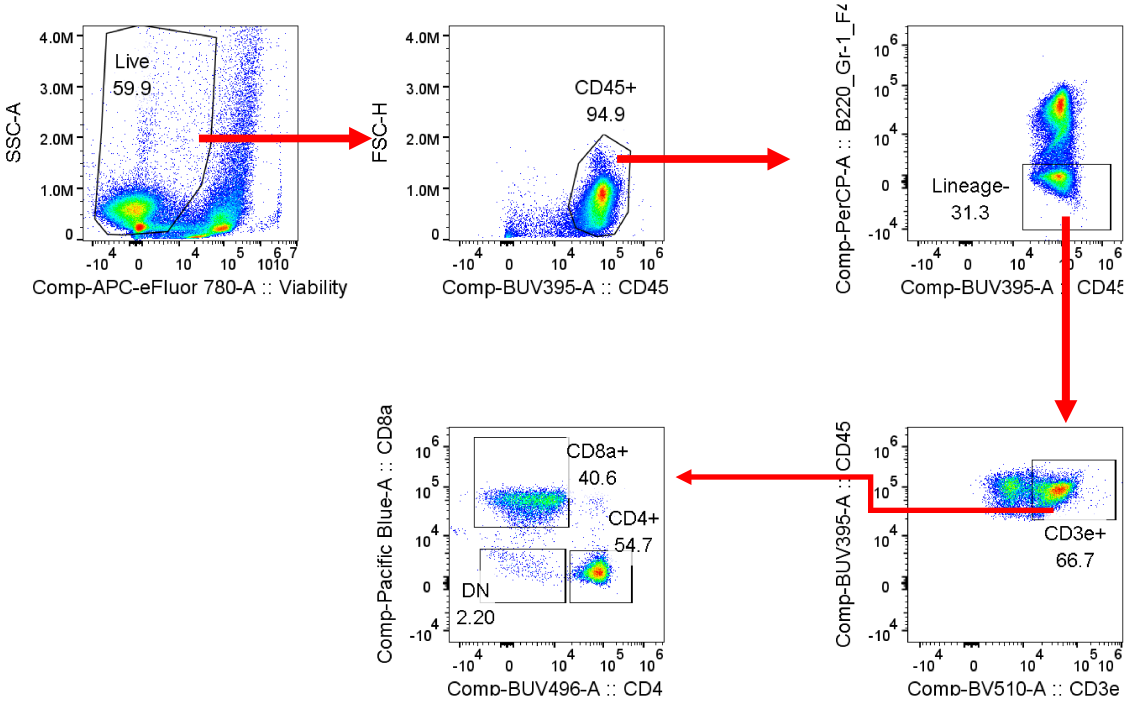
Live
59.9
SSC-A
Comp-APC-eFluor 780-A :: Viability
CD45+
94.9
FSC-H
Comp-BUV395-A :: CD45
Lineage-
31.3
Comp-PerCP-A :: B220_Gr-1_F4
Comp-BUV395-A :: CD45
CD3e+
66.7
Comp-BUV395-A :: CD45
Comp-BV510-A :: CD3e
CD8a+
40.6
CD4+
54.7
DN
2.20
Comp-Pacific Blue-A :: CD8a
Comp-BUV496-A :: CD4

Figure S12

Figure S12. Strategy to gate CD4 T and CD8 T cells and assess their activation profile. Single-cell suspensions from tumors and peripheral blood were analyzed for surface markers and nuclear transcription factors using spectral cytometry.CD45+ leukocytes were identified after gating out dead cells, followed by gating out B220+, Gr-1+, and F4/80+ cells (lineage-negative gating). Lineage-negative cells were further gated to identify CD4T and CD8 T cells to monitor surface and nuclear transcription factor expression profiles.

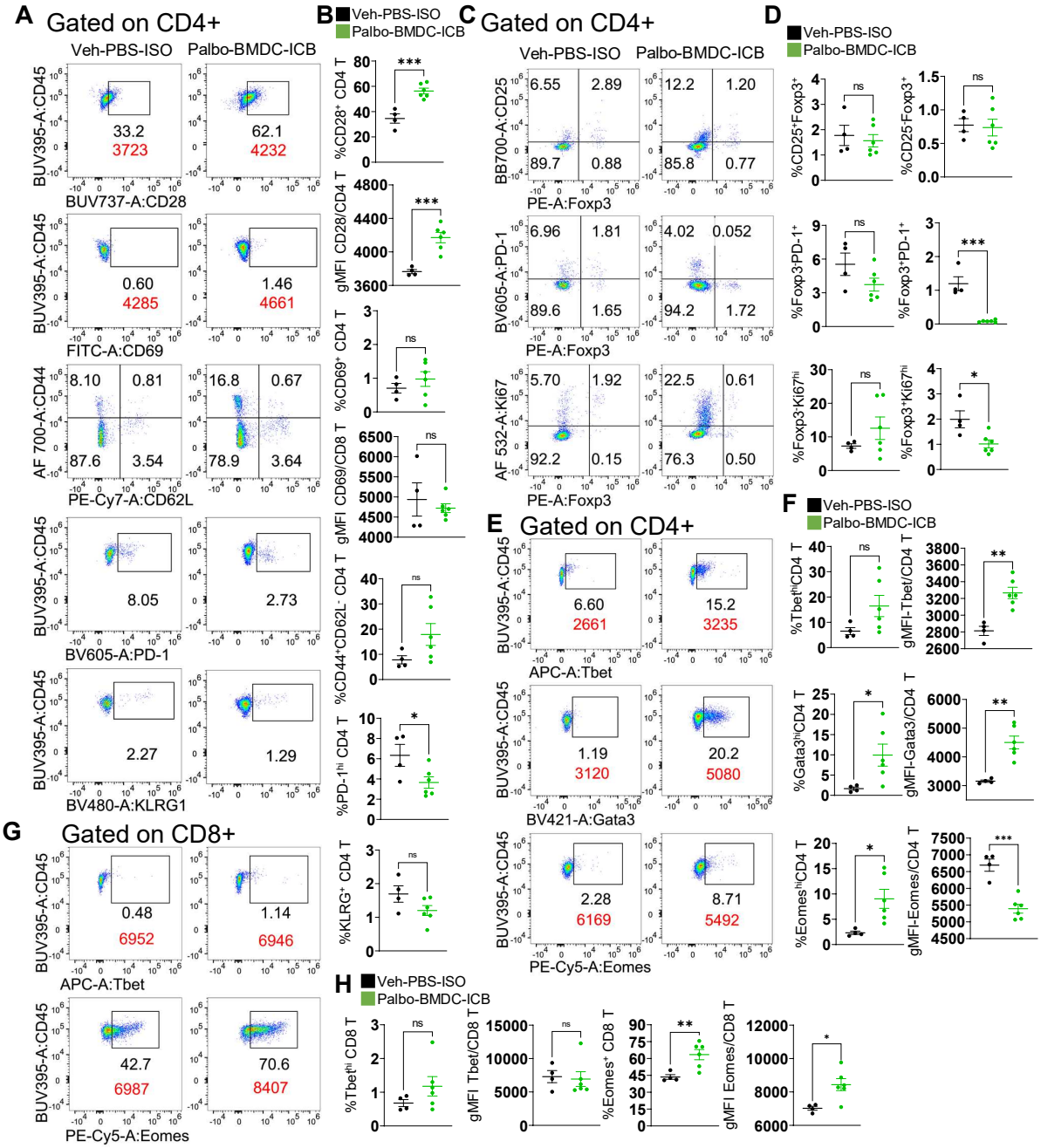
A
Gated on CD4+
Veh-PBS-ISO
Palbo-BMDC-ICB
BUV395-A:CD45
BUV737-A:CD28
33.2
3723
62.1
4232
0.60
4285
1.46
4661
FITC-A:CD69
AF 700-A:CD44
PE-Cy7-A:CD62L
8.10
0.81
87.6
3.54
16.8
0.67
78.9
3.64
BV605-A:PD-1
8.05
2.73
BV480-A:KLRG1
2.27
1.29
B
Veh-PBS-ISO
Palbo-BMDC-ICB
%CD28+ CD4 T
***
gMFI CD28/CD4 T
***
%CD69+ CD4 T
ns
gMFI CD69/CD8 T
ns
%CD44+CD62L- CD4 T
ns
%PD-1hi CD4 T
*
%KLRG+ CD4 T
ns
C
Gated on CD4+
Veh-PBS-ISO
Palbo-BMDC-ICB
BB700-A:CD25
PE-A:Foxp3
6.55
2.89
89.7
0.88
12.2
1.20
85.8
0.77
BV605-A:PD-1
6.96
1.81
89.6
1.65
4.02
0.052
94.2
1.72
AF 532-A:Ki67
5.70
1.92
92.2
0.15
22.5
0.61
76.3
0.50
D
Veh-PBS-ISO
Palbo-BMDC-ICB
%CD25+Foxp3+
ns
%CD25-Foxp3+
ns
%Foxp3+PD-1+
ns
%Foxp3+PD-1+
***
%Foxp3+Ki67hi
ns
%Foxp3+Ki67hi
*
E
Gated on CD4+
BUV395-A:CD45
APC-A:Tbet
6.60
2661
15.2
3235
BV421-A:Gata3
1.19
3120
20.2
5080
PE-Cy5-A:Eomes
2.28
6169
8.71
5492
F
Veh-PBS-ISO
Palbo-BMDC-ICB
%TbethiCD4 T
ns
gMFI-Tbet/CD4 T
**
%Gata3hiCD4 T
*
gMFI-Gata3/CD4 T
**
%EomeshiCD4 T
*
gMFI-Eomes/CD4 T
***
G
Gated on CD8+
BUV395-A:CD45
APC-A:Tbet
0.48
6952
1.14
6946
PE-Cy5-A:Eomes
42.7
6987
70.6
8407
H
Veh-PBS-ISO
Palbo-BMDC-ICB
%Tbethi CD8 T
ns
gMFI Tbet/CD8 T
ns
%Eomes+ CD8 T
**
gMFI Eomes/CD8 T
*

Figure S13

Figure S13. CDK4/6i, ICB, and BMDC therapy promotes CD4-Th1 and -Th2 immunity and increases the proportions of Tbet^{hi} and Eomes^{hi} CD8+ T cells in peripheral blood. A-H. Representative flow plots showing surface markers (**A, C, E**.) and graphs (**B, D, F**) showing differences in frequencies between the triple therapy and the control group. PYMT tumor-bearing mice were treated with palbociclib, BMDC, and anti-PD-1 and anti-CTLA4 antibodies as described in Fig. 5A; N=6) or mock treatment (vehicle, PBS, and isotype control antibodies; N=4). **G-H.** CD8 T cells were gated to identify Tbet^{hi} and Eomes^{hi} populations. Representative FACS plots (G) and graph (H) depict differences in frequencies between triple therapy and the control group. Statistical analysis in B, D, F and H was performed using a t-test. ns, not significant ($p \geq 0.05$), *p=0.01-0.05, **p=0.001-0.01, ***p=0.0001-0.001.

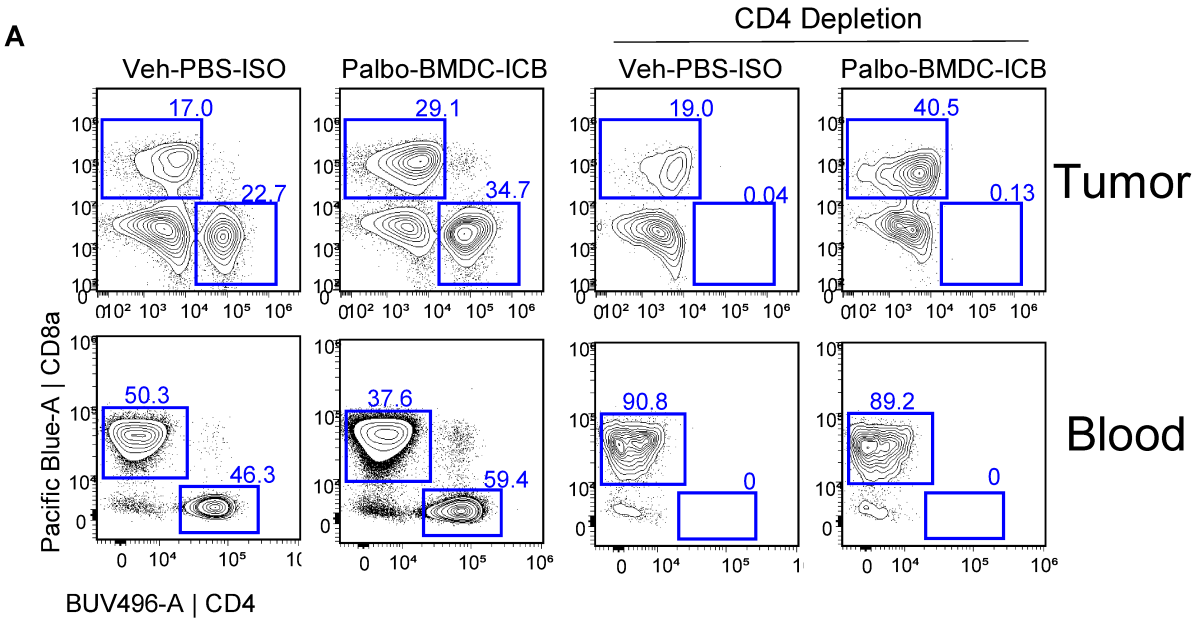
A
CD4 Depletion
Veh-PBS-ISO
Palbo-BMDC-ICB
Veh-PBS-ISO
Palbo-BMDC-ICB
17.0
22.7
29.1
34.7
19.0
0.04
40.5
0.13
Tumor
50.3
46.3
37.6
59.4
90.8
0
89.2
0
Blood
Pacific Blue-A | CD8a
BUV496-A | CD4

Figure S14

Figure S14. Analysis of CD4 T cell depletion efficiency. Single-cell suspensions from tumors and peripheral blood were analyzed by spectral cytometry. The gating scheme to identify $CD4^+$ and $CD8^+$ T cells is shown in **Fig. S9**. Representative dot plots indicate the mean percentages of CD4 T and CD8 T cells (N=3-6 mice per group).

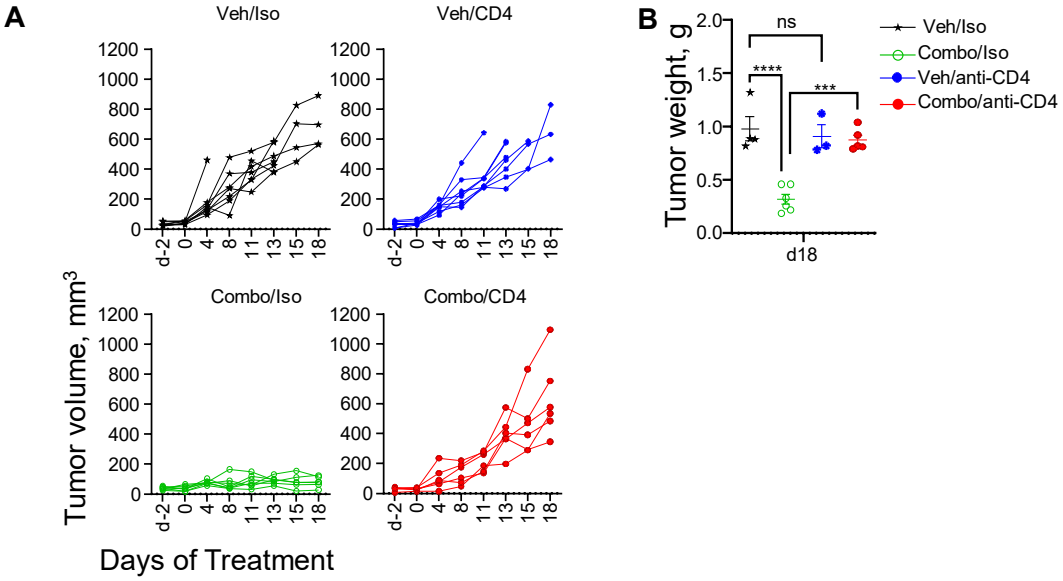
A
Veh/Iso
Veh/CD4
Combo/Iso
Combo/CD4
Tumor volume, mm3
Days of Treatment
B
Tumor weight, g
ns
****
***
d18
Veh/Iso
Combo/Iso
Veh/anti-CD4
Combo/anti-CD4

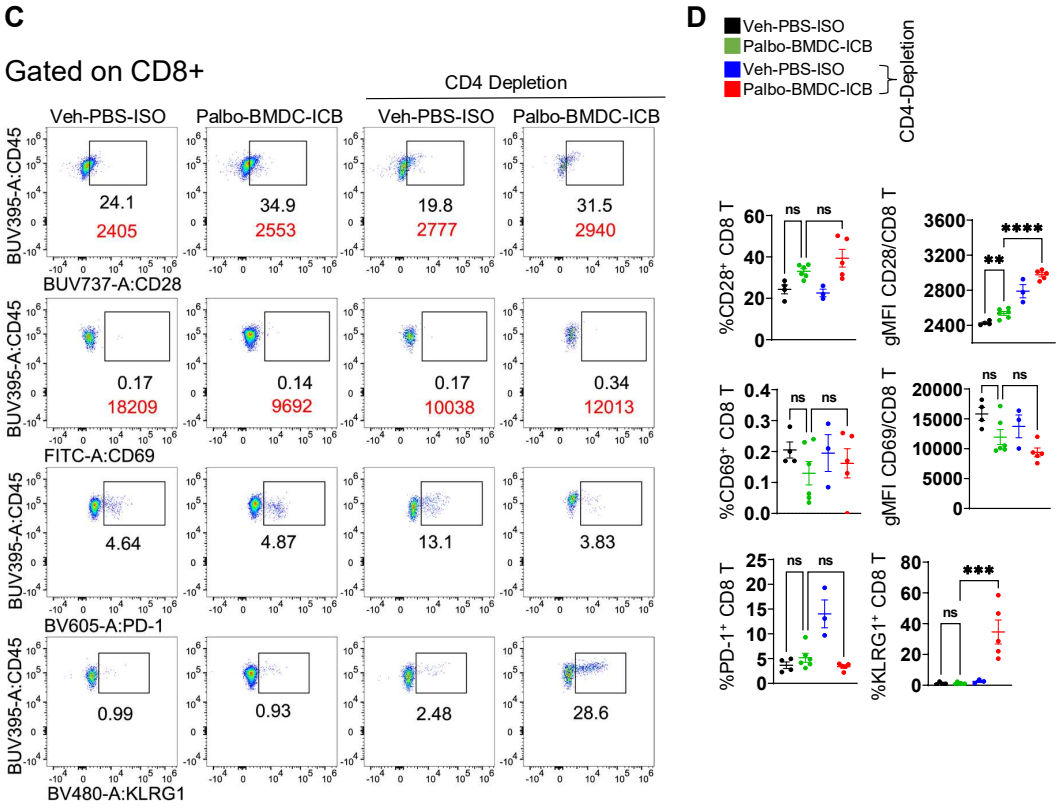
C
Gated on CD8+
CD4 Depletion
Veh-PBS-ISO
Palbo-BMDC-ICB
Veh-PBS-ISO
Palbo-BMDC-ICB
BUV395-A:CD45
BUV737-A:CD28
FITC-A:CD69
BV605-A:PD-1
BV480-A:KLRG1
24.1
2405
34.9
2553
19.8
2777
31.5
2940
0.17
18209
0.14
9692
0.17
10038
0.34
12013
4.64
4.87
13.1
3.83
0.99
0.93
2.48
28.6
D
Veh-PBS-ISO
Palbo-BMDC-ICB
Veh-PBS-ISO
Palbo-BMDC-ICB
CD4-Depletion
%CD28+ CD8 T
gMFI CD28/CD8 T
%CD69+ CD8 T
gMFI CD69/CD8 T
%PD-1+ CD8 T
%KLRG1+ CD8 T
ns
**
****
***

Figure S15

Figure S15. Depleting CD4 T cells in mice treated with CDK4/6i, BMDC and ICB abrogates tumor response. A. Spaghetti plot showing tumor volume change over time in PYMT tumor-bearing mice from the experiment shown in Fig 7A. N=6-8 mice per treatment group on d0-d13 and N=3-6 mice per treatment group on d15-d18. B. Tumor weight measurements on d18; N=3-6 mice per treatment group. Statistical comparison between treatment groups was performed using one-way ANOVA with Tukey's post-test with adjustment for multiple comparisons. C-D. Results of the flow cytometry of RBC lysed peripheral blood cells of mice treated with CDK4/6i, ICB, and BMDC therapy. Representative pseudocolor plots (C) from indicated treatment groups and graphs (D) show differences in frequencies of indicated cell populations. N= 3-6 mice per group. The p values were calculated using ANOVA with Tukey's post-test with adjustment for multiple comparisons. ns, not significant ($p \geq 0.05$), *p=0.01-0.05, ***p=0.0001-0.001, ****$p < 0.0001$.

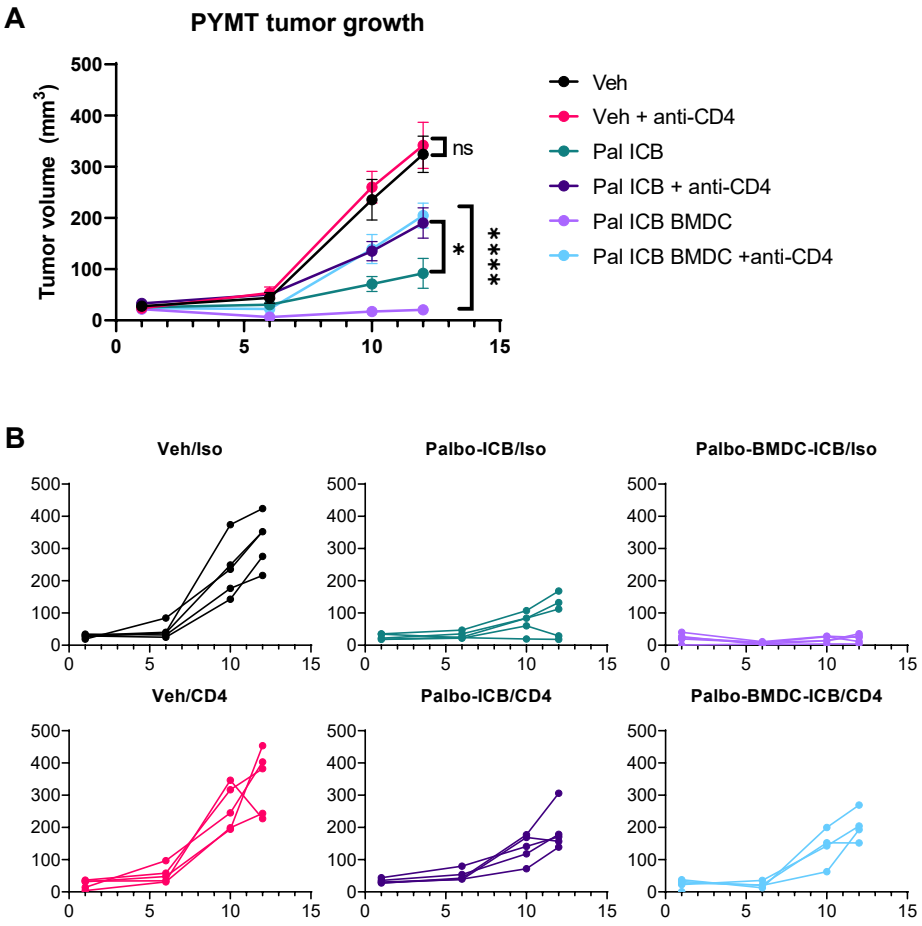
A
PYMT tumor growth
Tumor volume (mm3)
500
400
300
200
100
0
0
5
10
15
ns
*
****
Veh
Veh + anti-CD4
Pal ICB
Pal ICB + anti-CD4
Pal ICB BMDC
Pal ICB BMDC +anti-CD4
B
Veh/Iso
Palbo-ICB/Iso
Palbo-BMDC-ICB/Iso
Veh/CD4
Palbo-ICB/CD4
Palbo-BMDC-ICB/CD4

Figure S16

Figure S16. Depleting CD4 T cells in mice treated with CDK4/6i and ICB or CDK4/6i, BMDC and ICB abrogates tumor response. A-B. PYMT tumor bearing mice were treated as in Fig 7 except for addition of palbociclib and ICB group with or without CD4 depletion, N=4-5/treatment group. A Graph showing mean ± sem of tumor volume changes in groups. B. Spaghetti plot showing tumor volume changes of individual mice. Statistical analysis using mixed model with Dunnett's post-test was performed to compare tumor growth in different treatment groups. ns, not significant ($p \geq 0.05$), *p=0.01-0.05, ***p=0.0001-0.001, ****p<0.0001.

Table S1. Antibodies used for flow cytometry analysis.

S.NO.	Antigen	Antibody clone	Flurochrome	Vendor	Catalogue number
1	CD45.1	A20	APC	Biolegend	110714
2	CD45.2	104	BUV395	BD Biosciences	564616
3	TCRb	H57-597	BV510	BD Biosciences	563221
4	CD4	RM4-5	BUV496	BD Biosciences	741050
5	CD8	53-6.7	Pacific Blue	Biolegend	100725
6	B220	RA3-6B2	PE/Cy5	Biolegend	103209
7	NK1.1	PK136	PE/Cy7	Biolegend	108714
8	FoxP3	MF-14	PE	Biolegend	126404
9	CD24	M1/69	FITC	BD Biosciences	553261
10	PD-1	29F.1A12	PE-Dazzle 594	Biolegend	135228
11	Ki67	SolA15	Alexa Fluor 532	Invitrogen	58-5698-82
12	CD11b	M1/70	BV750	Biolegend	101267
13	CD11c	N418	BUV563	BD Biosciences	749040
14	Gr1	RB6-8C5	PerCP	Biolegend	108426
15	CD69	H1-2F3	BV605	Biolegend	104530
16	I-A/I-E	M5/114.15.2	AF700	Biolegend	107622
17	H-2Kb	AF6-88.5.5.3	eFluor710	ebiosciences	46-5958-82
18	CD103	M290	BV786	BD Biosciences	564322
19	CD86	PO3	BV650	BD Biosciences	740501
20	Viability	NA	efluor780	Invitrogen	50-112-9035
21	KLRG1	2F1	BV480	BD Biosciences	746353
22	CD80	16-10A1	BUV805	BD Biosciences	741956
23	CD45	30-F11	BUV395	BD Biosciences	564279
24	CD3	145-2C11	BV510	BD Biosciences	563024
25	B220	RA3-6B2	PerCP	Biolegend	103234
26	F4/80	BM8	PerCP	Biolegend	123126
27	CD69	H1-2F3	FITC	Invitrogen	11-0691-85
28	PD-1	29F.1A12	BV605	Biolegend	135220
29	CD62L	MEL-14	PE-Cy7	Biolegend	104418
30	CD25	PC61	BB700	BD Biosciences	566498
31	Tbet	4B10	APC	Biolegend	644814
32	Gata3	16E10A23	BV421	Biolegend	653814
33	Eomes	Dan11mag	PE-Cy5	Invitrogen	15-4875-80
34	CD28	37.51	BUV737	BD Biosciences	741720
35	HLA-DR	G46-6	BB515	BD Bioscience	564516
36	CD14	MΦP9	BB700	BD Bioscience	566465
37	CD16	B73.1	APC	BD Bioscience	561304
38	CD1c	F10/21A3	APC-R700	BD Bioscience	566615
39	CD123	6H6	BV421	BD Bioscience	567279
40	CD141	1A4	BV510	BD Bioscience	563298

41	Ki 67	B56	BV650	BD Bioscience	563757
42	CD11c	B-ly6	BV711	BD Bioscience	563130
43	CD3	UCHT1	PE-CF594	BD Bioscience	562280
44	CD19	HIB19	PE-CF594	BD Bioscience	562294
45	CD56	B159	PE-CF594	BD Bioscience	562289
46	CD86	2331	PE-Cy7	BD Bioscience	561128
47	Fixable Viability Stain 780			BD Bioscience	565388
48	Ter119	Ter119	PerCp	Biolegend	116226
49	NK1.1	PK136	PerCP	Biolegend	108726
50	B220	RA3-6B2	PerCP	Biolegend	103234
-51	Ly6G	1A8	PerCP	Biolegend	127654
52	CD172a (SIPRa)	P84	PE/Cy7	Biolegend	144008
53	XCR-1	ZET	PE/Dazzle 594	Biolegend	148233
54	CD117 (c-kit)	2B8	BV711	Biolegend	105835
55	CD115 (CSF-1R)	AFS98	BUV661	BD Biosceince	750949
56	CD135 (Flt3)	A2F10	PE/Cy5	Biolegend	135312
57	CD64	X54-5/7.1	PE	Biolegend	139304
58	CD14	Sa14-2	BV421	Biolegend	123329